# ALGORITHMS FOR AUTONOMOUS GPS ORBIT DETERMINATION AND FORMATION FLYING:

## *Investigation of Initialization Approaches and Orbit Determination for HEO*

**Summary of Research**

Principal Investigator: Penina Axelrad
Graduate Research Assistant: Eden Speed

Period Covered: 8/01/01-6/30/02

Colorado Center for Astrodynamics Research
University of Colorado, UCB 431
Boulder, CO 80309-0431

Grant No: NCC5-564

Report No: PA-02-170
Date: September 18, 2002

## ABSTRACT

This report summarizes the efforts to date in processing GPS measurements in High Earth Orbit (HEO) applications by the Colorado Center for Astrodynamics Research (CCAR). Two specific projects were conducted; initialization of the orbit propagation software, GEODE, using nominal orbital elements for the IMEX orbit, and processing of actual and simulated GPS data from the AMSAT satellite using a Doppler-only batch filter.

CCAR has investigated a number of approaches for initialization of the GEODE orbit estimator with little a priori information. This document describes a batch solution approach that uses pseudorange or Doppler measurements collected over an orbital arc to compute an epoch state estimate. The algorithm is based on limited orbital element knowledge from which a coarse estimate of satellite position and velocity can be determined and used to initialize GEODE. This algorithm assumes knowledge of nominal orbital elements, (a, e, i, $\omega$, $\Omega$) and uses a search on time of perigee passage ($\tau_p$) to estimate the host satellite position within the orbit and the approximate receiver clock bias. Results of the method are shown for a simulation including large orbital uncertainties and measurement errors.

In addition, CCAR has attempted to process GPS data from the AMSAT satellite to obtain an initial estimation of the orbit. Limited GPS data have been received to date, with few satellites tracked and no computed point solutions. Unknown variables in the received data have made computations of a precise orbit using the recovered pseudorange difficult. This document describes the Doppler-only batch approach used to compute the AMSAT orbit. Both actual flight data from AMSAT, and simulated data generated using the Satellite Tool Kit and Goddard Space Flight Center's Flight Simulator, were processed. Results for each case and conclusion are presented.

**Contents**

## INITIALIZATION ALGORITHM

### 1. Introduction

The GPS Enhanced Orbit Determination flight software (GEODE) was developed by Goddard Space Flight Center as a robust method for real-time orbit determination using the Global Positioning System. GEODE is a sequential filter designed to process GPS pseudoranges and Doppler measurements from any number of satellites, with a dynamic model to determine an estimate of the host vehicle orbit. The vehicle state is represented by position and velocity coordinates in an earth-centered inertial frame (ECI).

In low earth orbit (LEO) it is possible to initialize the GEODE state vector using a point solution - i.e. an instantaneous solution for position and velocity based on four or more simultaneous pseudorange and Doppler measurements. If the state estimate is within a few kilometers of the true position, GEODE has been shown to consistently converge to an improved orbit solution within one orbit. This is not the case in high earth orbits or highly elliptical orbits, where there are rarely, if ever, sufficient satellites visible for a point solution. In these situations a different initialization approach is required. Furthermore, even in LEO, the requirement for a point solution can delay the initialization of GEODE because of the need to perform a cold start/blind search for the satellite signals.

The objective of our research has been to develop a robust method to initialize GEODE under the conditions expected in LEO and HEO. The basic assumption was that a batch approach was required to gather measurements over an arc of the orbit to produce an epoch state estimate sufficiently accurate to initialize GEODE. To provide a very robust approach, we assume only that the initialization algorithm has knowledge of the nominal orbital parameters for the vehicle. We then use typical launch vehicle orbit injection errors as the bounds for the errors in these starting points. We considered various parameterizations of the initialization batch and both search techniques and iterative batch schemes.

This document reviews the method used for this approach and presents the mathematical algorithms involved. Results from several test cases are also presented, as well as suggestions for future study.

## 2. Approach

The most obvious approach to initialization of GEODE would be to perform a batch solution for the position and velocity in ECI at a reference time. This has a straightforward relationship to the GPS pseudorange and Doppler measurements and directly produces the initial state estimate for GEODE. Unfortunately, there is no good way to construct this initial estimate of position and velocity. (Note: Earthbound users can assume an initial position at the center of the earth and achieve rapid convergence of a point solution approach). Furthermore, in order to tie together the time sequence of measurements for the batch, an orbit propagator must be used. The critical relationships among uncertainties in position and velocity elements within an orbit are not well captured by the ECI representation. In fact, in our initial investigation we found that an initialization based upon position and velocity vectors is very sensitive to uncertainties and does not provide a robust approach.

A better method, based upon an orbit element representation, relies upon constraints of the orbital dynamics to narrow the range of possible initial conditions. This type of approach was selected based on the fact that the nominal orbital elements are well known and highly constrained by the launch trajectory. In addition, standard injection errors associated with these elements can be estimated based on the vehicle design and history. The advantage with this method is that the orbit errors provide far more geometric information than do the classical position and velocity error expressions. In particular, the angular position of the orbit (inclination, node, and argument of perigee), and orbital energy are very constrained by the launch; whereas the position of the vehicle within the orbit plane is not at all known. The values for the semi-major axis and eccentricity are somewhere in the middle, qualitatively, in terms of a priori knowledge.

To describe the method clearly in the following section, we will use a classical orbit element representation and assume purely Keplerian motion. However, for the actual implementation

proposed for GEODE we outline the steps for an equinoctial representation using the dynamic propagation routines built into GEODE.

### 2.1 Parameters

For our development and initial testing of the initialization approach we parameterized the orbit using classical orbital elements (a, e, i, $\Omega$, $\omega$, and $\tau_p$). The first five elements define the geometry of the orbit with the nominal values for these parameters specified at launch. The final parameter, time of perigee passage ($\tau_p$), together with the current time, prescribes the position of the vehicle within the orbit. This value is not well known ahead of time. So, the goal of the initialization process is to identify the correct $\tau_p$ and compute a position and velocity estimate for the satellite at the filter start time. We considered both HEO and LEO orbits.

### 2.2 Measurements

We assume that the onboard GPS receiver acquires and tracks as many satellites as possible using a cold start or blind search technique. The receiver is assumed to form both pseudorange and Doppler measurements, and to collect the broadcast GPS satellite ephemeris data from the visible satellites. In HEO orbits, this visibility can be reduced to zero for extended periods of time as the host vehicle orbits above the GPS constellation. We assume that measurements are provided at 1 minute intervals, and consider solutions including pseudorange and/or Doppler.

Time onboard the spacecraft is assumed to be known to within 1 second after acquisition and tracking of the first GPS satellite. A clock bias of up to 1 second may still be present, but the a priori estimate is set to zero. The stability of the clock is assumed to be $1/10^{10}$. This means that over a 12 hour period the change in the clock bias is within 5 μs. The overall clock bias is quite large (~ 3 x $10^8$ m) but the drift error is less than 1 m/s. The large bias dominates the pseudorange residuals, but we will show later that by comparing residuals for different satellites we can still compute a reliable initial condition using these measurements. If measurements from only one satellite are available it is not always possible to isolate the correct starting point in the orbit if there is a large clock bias.

### 2.3 Data Arc

We considered various data arc lengths including 10 minutes, 100 minutes, and 600 minutes for the HEO orbit, and 10 minutes, 50 minutes, and 100 minutes for the LEO case, with measurements provided every 60 seconds. We also adjusted the starting point within the orbit to evaluate data arcs at perigee, apogee, and intermediate points. This provides a wide range of visibility and geometric conditions.

### 2.4 Batch Solution

The algorithm assumes knowledge of the orbital elements, (a, e, i, $\Omega$, $\omega$), and performs a search to estimate the remaining unknown – the location within the orbit, characterized by $\tau_p$. To process all the measurements in a batch solution, the nominal host vehicle elements are used to predict the vehicle position and velocity at each of the measurement times. For our initial investigation the propagation is though a purely Keplerian model with no perturbation effects.

Combining the host vehicle position and velocity predictions with GPS satellite positions computed from the broadcast ephemerides, we compute the expected pseudorange and/or Doppler measurements. These are compared to the measurements from the receiver and the residuals for the entire data arc are tallied.

The characteristics of the measurement residuals for the batch indicate which $\tau_p$ is correct. For Doppler measurements and for PR measurements without clock biases, the RMS of the residuals is unambiguously smallest for the correct position within the orbit plane. In the presence of a large clock bias there is an offset in the residuals that prevents the use of a simple RMS evaluation. When observations are available from more than 1 satellite within the batch, the correct $\tau_p$ can be identified by the minimum standard deviation of the measurement residuals. This will be illustrated in the results shown in the following section. Thus, we compute the mean and standard deviation of the residuals for all measurements in the batch. The value of $\tau_p$ that minimizes the residual standard deviation locates the correct

host vehicle position within the orbit. The mean of the residuals for this $\tau_p$ provides a coarse estimate of the receiver clock bias. The position and velocity estimates can then be produced for the current time based upon the nominal elements and the optimal $\tau_p$.

The algorithm starts with a course search in $\tau_p$, searching in increments of one tenth of an orbit. This search increment can then be refined to smaller resolutions to gain a better initial estimate of position. This is ultimately limited by the uncertainty in the nominal elements. To provide a general approach for different types of orbits, the current search implementation increments by fractions of an orbit period that correspond roughly to tens of minutes, one minute, and less than one second for both HEO and LEO orbits. In particular, we use 1/10, 1/100, and 1/10000 of an orbit for the LEO case, 1/10, 1/1000 and 1/100000 of an orbit in the HEO case. The figures in the following sections show that the search space is well defined for data arcs of 100 min or longer eliminating the possibility of searching in a false null region. For initialization near perigee, data arcs as short as 10 min are adequate.

### 2.5 Computation of the Initial State Estimate

Once the best $\tau_p$ ($\tau_p^*$) is found, the position and velocity of the host at a reference time are computed based on the assumed elements and $\tau_p^*$. The initial estimate of the clock bias may be taken as the mean of the pseudorange residuals for the minimum $\sigma_{\delta\rho}$ residual solution. The initial covariance matrix may also be computed from the launch uncertainties.

## 3. Simulation

To evaluate the initialization approach prior to implementation in the GEODE code, we used a Matlab simulation environment. The components of the simulation are described in the following subsections.

### 3.1 Truth Model

We use M. Moreau's Matlab codes to establish the truth model for evaluating the algorithms. This includes 3 basic steps:

a) Define host vehicle orbit (R,V, and orbit elements based on Keplerian model) and visibility conditions (antenna masking)

b) Define GPS satellite orbits (R,V computed from broadcast message file) and visibility conditions (antenna gain pattern)
c) Compute range, range rate, and visibility (including antenna masking, gain patterns and Earth blockage) at 1 minute increments

### 3.2 Measurement Model

To produce measurements for the initialization algorithm we do the following:

a) Select data batch (start and end times). Set the reference time to the start of the data batch. This insures that orbits are not propagated over very long intervals.
b) Determine number of satellites observed and number of measurements per satellite for the entire arc.
c) Produce error corrupted pseudorange and Doppler measurements. We add a large pseudorange bias (3e8 m) to all the measurements and a random error to each measurement (Gaussian with $\sigma$=20m). Both the random error and bias are quite conservative. A random error is also added to each Doppler measurement (Gaussian with $\sigma$ = 5 m/s)

### 3.3 Initialization algorithm

a) Set up nominal orbit elements given standard injection errors.
b) Search $\tau_p$ over 1 orbit, incrementing in fractions of an orbit.
For each $\tau_p$:

At each measurement time in the batch:

i). Compute position and velocity estimate based on nominal orbital elements and the current $\tau_p$ value.

$$(a_{error}, e_{error}, i, \Omega, \omega, \tau_p, t_{meas}) \rightarrow (R, V)_{estimated\ at\ t_{meas}}$$

ii). Compute expected measurements and line of sights. Incorrect time estimates offset by one second are utilized for computing GPS satellite locations.

Estimated LOS:

$$LOS_{est} = R_{GPS\,truth} - R_{SAT\,est}$$

Estimated Range:

$$\rho_{est} = \sqrt{LOS_{est}^2}$$

Estimated Range-rate:

$$\dot{\rho}_{est} = \left(\frac{LOS_{est}}{\rho_{est}}\right)\left(V_{GPS\,truth} - V_{SAT\,est}\right)$$

iii). Compute PR and/or Doppler residuals. These are accumulated over the batch for each $\tau_p$.

$$Meas\,\mathrm{Re}sidual = [\rho_{meas} - \rho_{est}, \dot{\rho}_{meas} - \dot{\rho}_{est}]$$

$$SSR = SSR + MEAS_{\rho}^{2}$$

$$SSRdop = SSRdop + MEAS_{\dot{\rho}}^{2}$$

iv). The standard deviation and the mean of the measurement residuals are determined for each $\tau_p$

c) Compute $R_{est}$, $V_{est}$ at reference time using best estimated $\tau_p$ and nominal orbital elements.

### 3.4 Performance Analysis

a. Evaluate metric for $\tau_p$ search to see if any false nulls occur
b. Evaluate error in estimated R, V at the reference time to see if sufficient for GEODE initialization.

### 3.5 Position and Velocity Calculation:

Estimated orbital elements, (a, e, i, Ω, ω, $\tau_p^*$), are converted to position and velocity estimates for direct comparison with the truth orbit.

1. Input orbital elements with injection errors, best estimate of $\tau_p$, reference time.
2. Calculate $(R, V)_{est}$ at reference time:

$$(a_{error}, e_{error}, i, \Omega, \omega, \tau_{p\,est}, t_{meas}) \rightarrow (R_t, V_t)_{est}$$

3. Compare truth position and velocity with estimated position and velocity

$$R_{diff\ xyz} = R_{truth} - R_{est}$$

$$V_{diff\ xyz} = V_{truth} - V_{est}$$

Compare truth position and velocity with estimated position and velocity in RIC coordinates

a. Transform matrix from truth positions and velocities

$$R = \frac{\vec{R}_{truth\ xyz}}{\left|\vec{R}_{truth\ xyz}\right|}$$

$$W = \frac{\vec{R}_{truth\ xyz} \times \vec{V}_{truth\ xyz}}{\left|\vec{R}_{truth\ xyz} \times \vec{V}_{truth\ xyz}\right|}$$

$$S = W \times R$$

$$T_{ric}^{\ xyz} = \begin{bmatrix} R(1) & R(2) & R(3) \\ S(1) & S(2) & S(3) \\ W(1) & W(2) & W(3) \end{bmatrix}$$

b. Compute position and velocity differences in RIC frame

$$R_{diff\ ric} = T_{ric}^{xyz}\ R_{diff\ xyz}$$

$$V_{diff\ ric} = T_{ric}^{xyz}\ V_{diff\ xyz}$$

1. Compute minimum position and velocity differences in XYZ, and RIC frames

## 4. Results

To evaluate the algorithm we considered an ISS (LEO) and IMEX (HEO) orbit. Table 1 summarizes the simulation parameters and the errors considered. Two test scenarios with different orbit injection errors were considered for each type of orbit. We evaluated start times at perigee and apogee of the orbit using data arcs of 10 min, 100 min, and 600 min for the HEO orbit, and 10 min, 50 min and 100 min for the LEO orbit.

**Table 1. Simulation Parameters and Error Models**

| | |
|---|---|
| Orbits | |
| ISS (LEO) (6415 km x 7091 km, 92 min period) | |
| IMEX (HEO) (6729 km x 42164 km, 633 min period) | |
| Keplerian orbit propagation | |
| Orbit injection errors | |
| *Scenario 1* | *Scenario 2* |
| perigee altitude: + 1 km | perigee altitude: + 1 km |
| apogee altitude: + 100 km | apogee altitude: + 10 km |
| inclination: + 1 degree | inclination: + 1/10 degree |
| nodes: + 1 degree | nodes: + 1/10 degree |
| Measurement errors | |
| Receiver clock bias – 0 s, 0.1 s, 1 s | |
| Pseudorange – random Gaussian error ($\sigma$ = 20) | |
| Doppler – random Gaussian error ($\sigma$ = 5) | |
| Data arcs | |
| HEO: | |
| Starting point – perigee (t = 1 or t = 633), apogee (t = 318 min), intermediate (t = 200 min) | |
| Arc length – 10 min, 100 min, 600 min | |
| LEO: | |
| Starting point- perigee (t = 1), near apogee (t = 100), intermediate (t = 50) | |
| Arc length - 10 min, 50 min, 100 min LEO | |

Satellite visibility and altitude for the two orbits are shown in Figures 1 and 2, provided by M. Moreau's visibility simulations. Data arcs and start times for each orbit type are also highlighted.

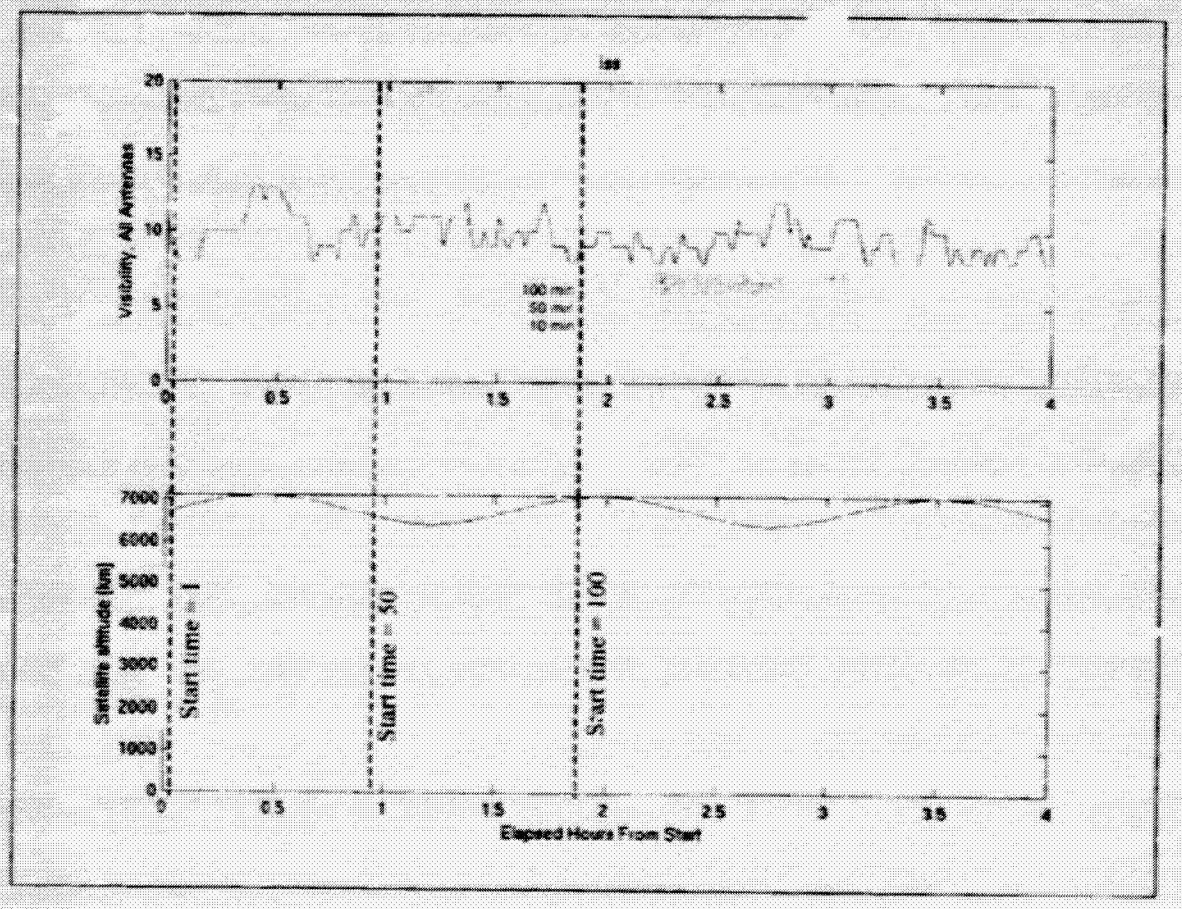


**Figure 1: ISS Visibility, Data Arcs and Start times.**

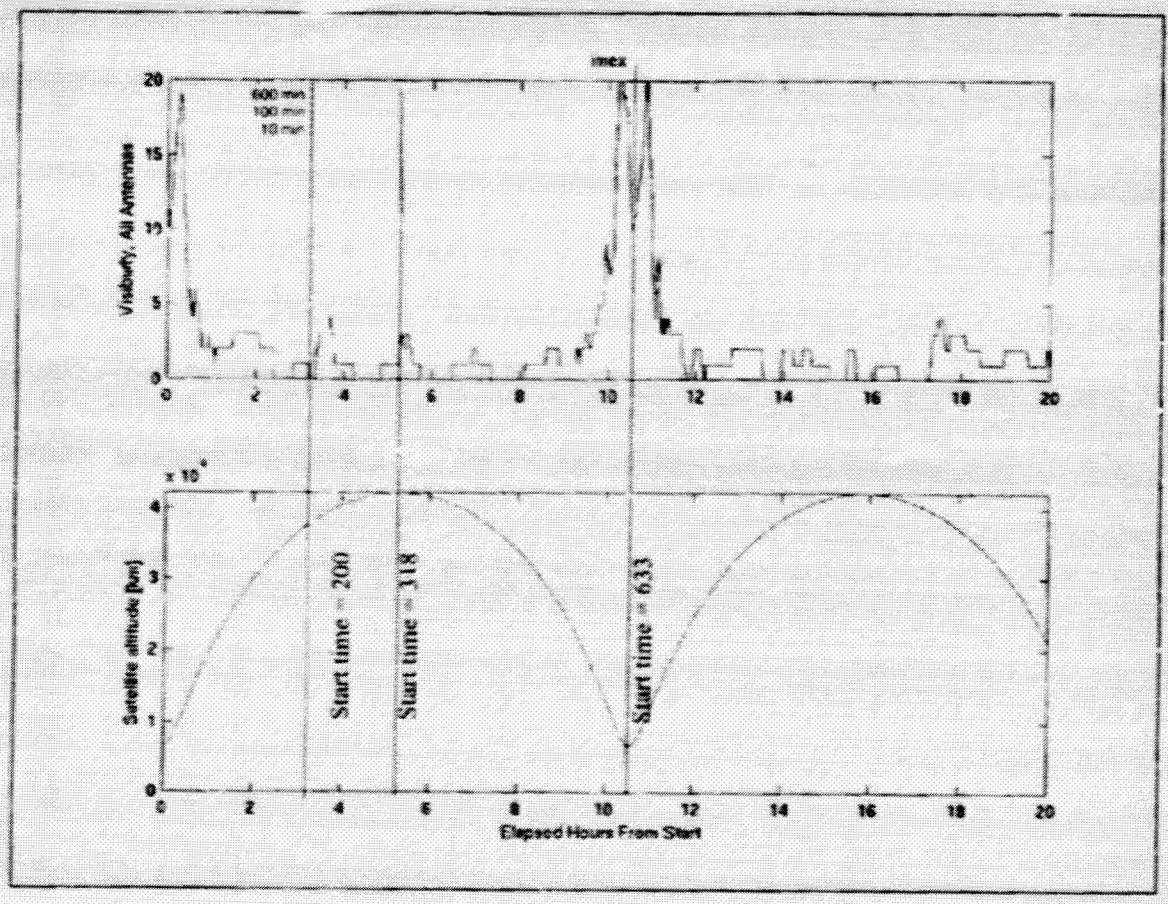


**Figure 2: IMEX Visibility, Data Arcs and Start times.**

### 4.1 Simulation Results for ISS Initialization

Figures 3 -5 show the $\tau_p$ search results for the ISS orbit given the larger injection errors presented in scenario 1. Measurement residuals are computed for $\tau_p$ values spaced at 0.1 orbit (approximately 10 minute) increments. The graphs each include curves for several starting points and data arc lengths. Figures 3 (a) and (b) show the $\tau_p$ dependence of the RMS residuals for pseudorange and Doppler, respectively, in the case of no clock bias. Figure 4 gives the RMS error of the pseudorange residuals with a 1 s clock error, and Figure 5 shows the mean and standard deviation of the pseudorange residuals for this case.

From Figure 3 one can see that even data arcs as short as 10 min give a reliable minimum RMS residual at the correct $\tau_p$ in the absence of a large clock bias. However, Figure 4 shows that the RMS residual is not reliable when large clock biases are present. Thus, we rely upon the standard deviation of the range residuals, shown in Figure 5b. The approximate clock bias value can be obtained as the mean value at $\tau_p^*$ shown in Figure 5a. For example, the 100 min data arc starting at 50 gives a clock bias estimate of 0.9960 seconds (2.9881 0e8 m).

Figure 6 shows the RMS pseudorange and Doppler residuals for the narrower search on $\tau_p$ in 1 s increments, over the region centered on the minimum value from the coarse search. The clock bias from the coarse search is included in the estimate. The minimum RMS value locates $\tau_p^*$ to within 1 s.

Using the a priori orbital elements and the derived $\tau_p^*$, the position and velocity of the host vehicle at the epoch are determined. Table 2 summarizes the errors in the epoch state estimate for the ISS orbit given the injection errors of scenario 1. Additionally, Table 3 summarizes the errors in the epoch state estimate from scenario 2 test runs. Values are given for $\tau_p$ resolution of 1s up to 10 min.

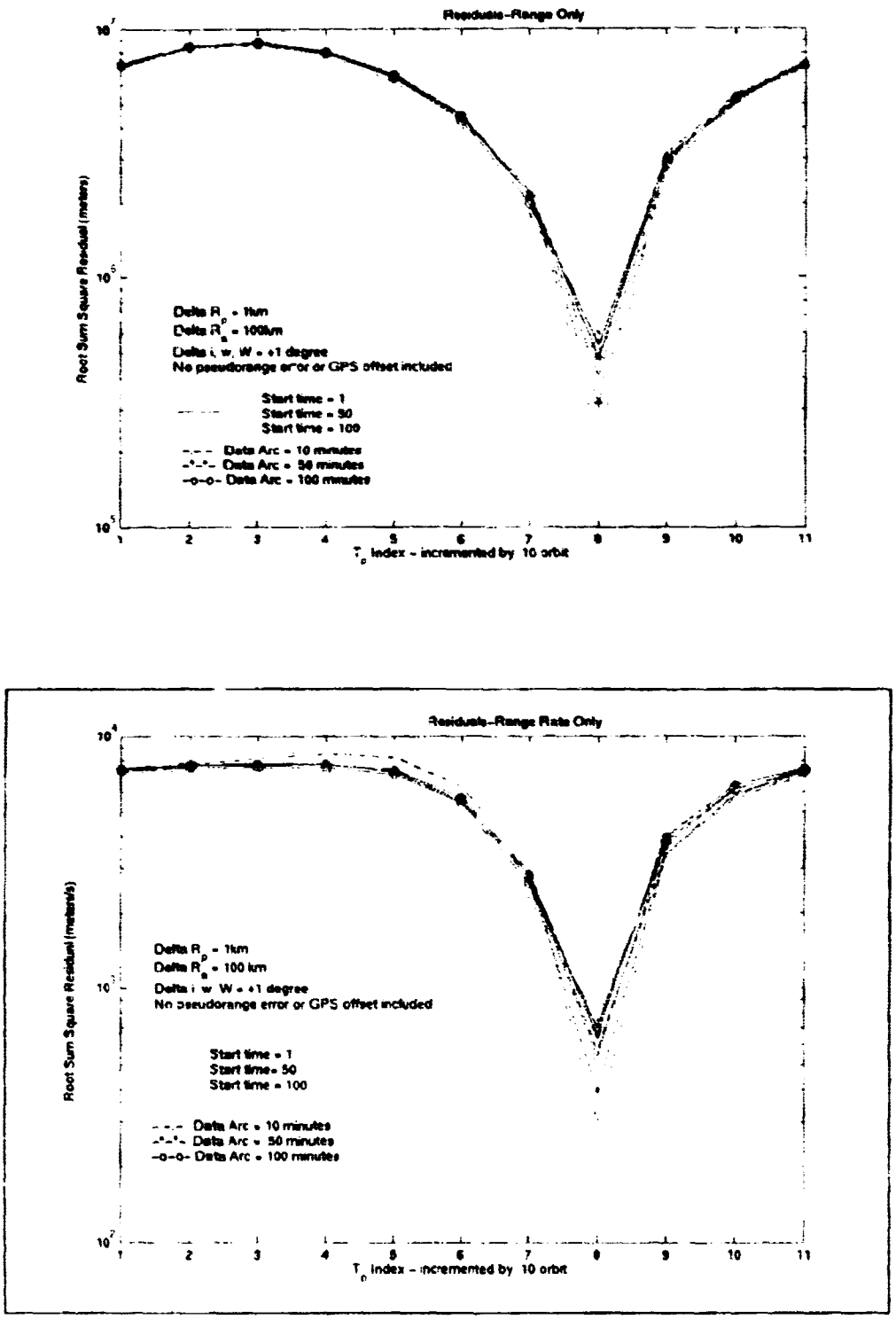


**Figure 3a and 3b: RSS Residuals for ISS Orbit with No Clock Bias.** Graphs show multiple start times and data arcs for range residuals (top) and range rate residuals (bottom) as a function of the assumed $\tau_p$.

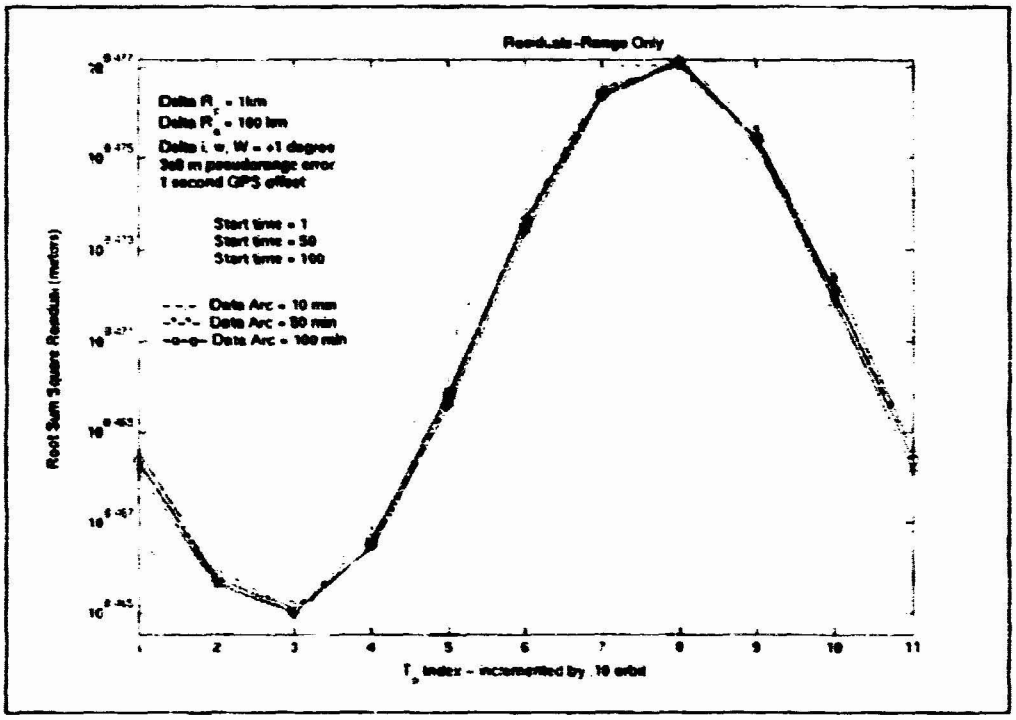


**Figure 4: RSS Residuals for ISS Orbit with 1 s Clock Bias.** Graphs show multiple start times and data arcs for range residuals as a function of the assumed $\tau_p$.

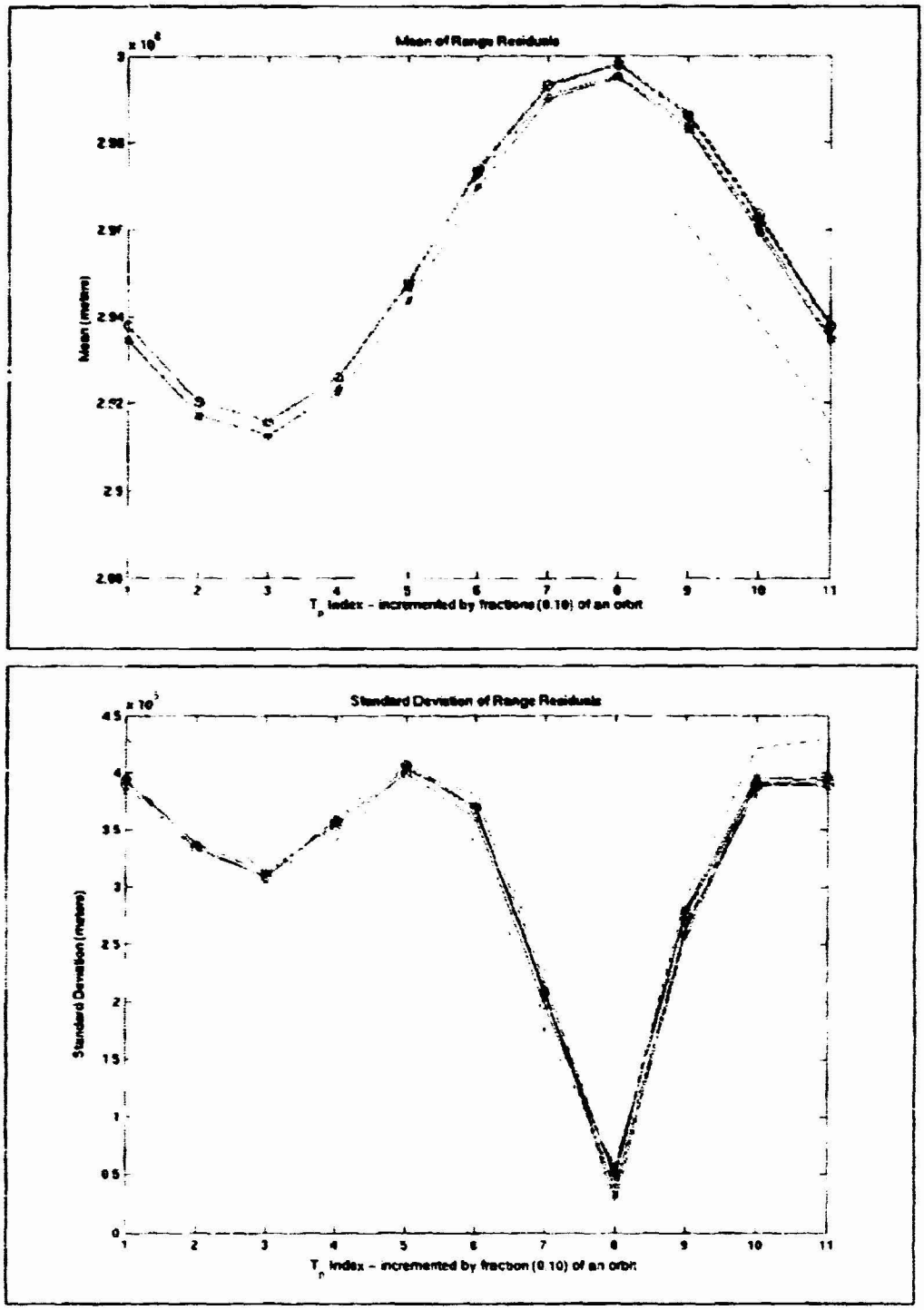


**Figure 5a and 5b: Mean and Standard Deviation of Range Residuals for ISS Orbit with 1 s Clock Bias.** Graphs show multiple start times and data arcs for range residuals as a function of the assumed $\tau_p$. Top is the mean of the residuals for each $\tau_p$, and bottom graph is the standard deviation of the residuals for each $\tau_p$.

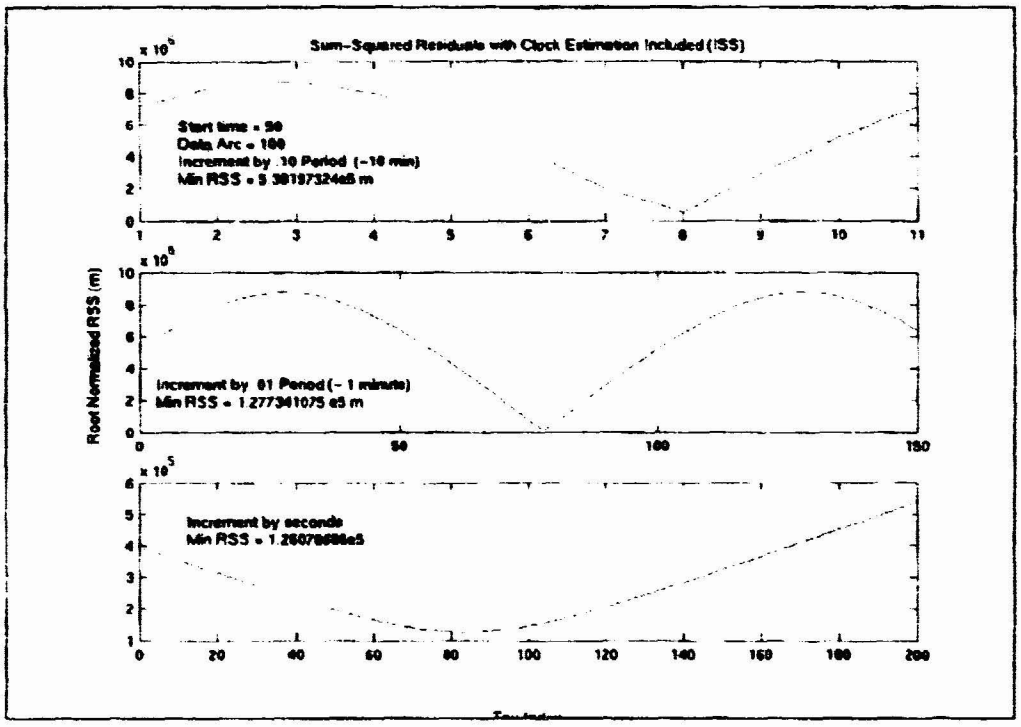


**Figure 6: RMS Range Residuals Over Narrow Search with Estimated Clock**. Depicted are iterations on $\tau_p$ with intervals from 1/10 an orbit (approximately 10 minutes) to one second.

**Table 2: ISS Position and velocity estimation errors for batch initialization.** Initialization includes nominal orbit injection errors given in Table 1 for scenario 1. Results are shown for data arcs at perigee and apogee. Position and velocity errors in radial, in-track, and cross-track directions are given for the end of the data arc (100 minutes). The correct time of perigee passage is 4342 s.

| | Perigee data arc (1038 measurements) | | | Apogee data arc (982 measurements) | | |
|---|---|---|---|---|---|---|
| Search Increment | Tau Error (s) | Position Error RIC (m) | Velocity Error RIC (m/s) | Tau Error* (s) | Position Error RIC (m) | Velocity Error RIC (m/s) |
| 0.1 orbit (552.3 s) | 126.32 | R = 3.76e4<br>I = 8.03e5<br>C = 1.41e5 | R = 9.45e2<br>I = 87.37<br>C = 70.91 | 126.32 | R = 2.17e4<br>I = 1.28e6<br>C = 1.34e5 | R = 1.46e3<br>I = 1.57e2<br>C = 64.138 |
| 0.01 orbit (55.2 s) | 14.61 | R = 5.53e4<br>I = 3.34e4<br>C = 1.48e5 | R = 14.17<br>I = 35.13<br>C = 51.25 | 14.61 | R = 4.24e4<br>I = 4.16e5<br>C = 1.409e5 | R = 4.27e2<br>I = 30.72<br>C = 43.50 |
| 0.0001 orbit (0.55 s) | 4.19 | R = 5.84e4<br>I = 1.21e5<br>C = 1.49e5 | R = 72.98<br>I = 36.04<br>C = 49.38 | 10.149 | R = 4.26e4<br>I = 3.81e5<br>C = 1.41e5 | R = 3.86e2<br>I = 28.29<br>C = 42.64 |

**Table 3: ISS Position and velocity estimation errors for batch initialization.** Initialization includes nominal orbit injection errors given in Table 1 for scenario 2. Position and velocity errors in radial, in-track, and cross-track directions are given for the end of the data arc (10 min).

| | Perigee data arc (96 measurements) | | | Apogee data arc (113 measurements) | | |
|---|---|---|---|---|---|---|
| Search Increment | Tau Error (s) | Position Error RIC (m) | Velocity Error RIC (m/s) | Tau Error* (s) | Position Error RIC (m) | Velocity Error RIC (m/s) |
| 0.1 orbit (552.3 s) | 82.068 | R = 4.08e4<br>I = 5.52e5<br>C = 1.49e4 | R = 6.20e2<br>I = 29.08<br>C = 4.08 | 82.068 | R = 2.99e3<br>I = 6.28e5<br>C = 1.43e4 | R = 7.28e2<br>I = 36.29<br>C = 2.42 |
| 0.01 orbit (55.2 s) | 26.76 | R = 1.046e3<br>I = 2.39e5<br>C = 1.51e4 | R = 1.59e2<br>I = 5.91<br>C = 3.07 | 26.76 | R = 8.72e3<br>I = 1.92e5<br>C = 1.45e4 | R = 2.29e2<br>I = 4.56<br>C = 1.30 |
| 0.00001 orbit (0.55 s) | 8.516 | R = 6.48e3<br>I = 2.57e3<br>C = 1.52e4 | R = 7.42<br>I = 4.35<br>C = 2.74 | 3.539 | R = 3.82e3<br>I = 7.93e3<br>C = 1.44e4 | R = 4.78<br>I = 1.279<br>C = .829 |

**Simulation Results for IMEX Initialization**

Similar results are given for the elliptical IMEX orbit. Figures 7 (a) and (b) show the range and Doppler RMS residuals for several start times and data arcs, without clock bias. $\tau_p$ values are spaced at 0.1 orbit (63 min) increments. Figures 8 and 9 give the RSS, mean and standard deviation of the pseudorange residuals with a 1 s clock error.

Figures 7 (a) and (b) show that for a course search without clock bias, the correct $\tau_p^*$ can be derived from the single minimum from both range and range-rate data. However, further examination at smaller search increments (10 minutes), the geometry of the range-rate data at apogee for data arcs of less than 600 minutes becomes insufficient for a single minimum search.

As indicated in the ISS trials, the addition of a 1 second clock bias eliminates the possibility of using the RMS error to find the correct $\tau_p^*$. However, from Figure 9(b) one can see that the correct minimum can be located for long data arcs (approximately 600 minutes) and for start times near perigee. The geometry for short data arcs, especially near apogee, may still be insufficient for locating the correct $\tau_p^*$. From Figure 9 (a), an approximate clock bias value of 0.98505 sec (approximately 2.95 meters) can be determined.

Using the nominal orbital elements and the derived $\tau_p^*$ value, the position and velocity of the host vehicle at the epoch are determined and compared with truth values. Tables 4 and 5 summarize the errors determined for the IMEX orbit in RIC coordinates for scenarios 1 and 2 respectively. Uncertainties in the inclination and node elements negatively impact the accuracy of the $\tau_p^*$ found within the search. This error in $\tau_p^*$ significantly reduces the accuracy of the position and velocity estimates.

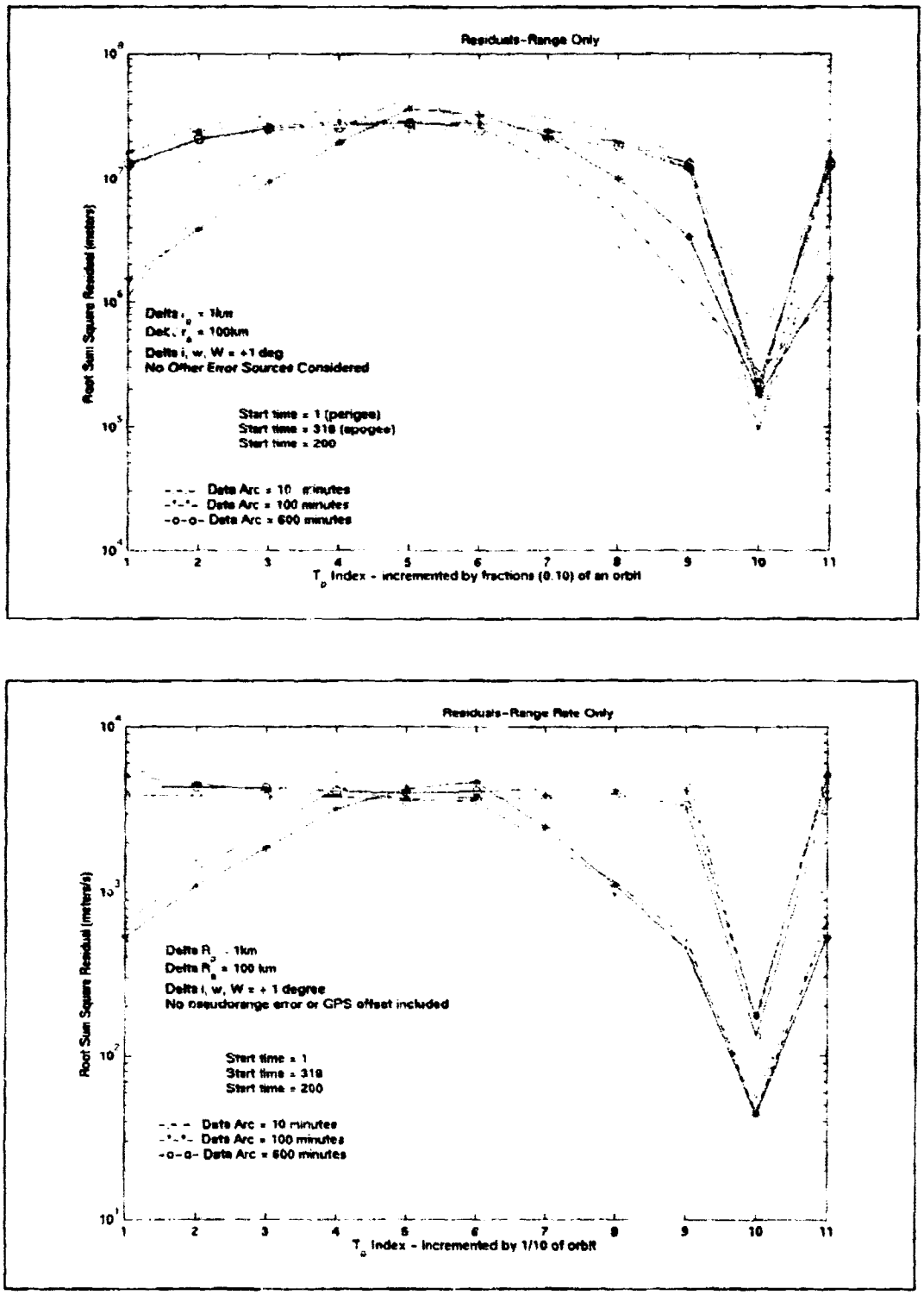


**Figure 7a and 7b: Multiple Start time/Data Arc for IMEX case.** Graphs show multiple start times and data arcs for range residuals (top) and range rate residuals (bottom) as a function of the assumed $\tau_p$.

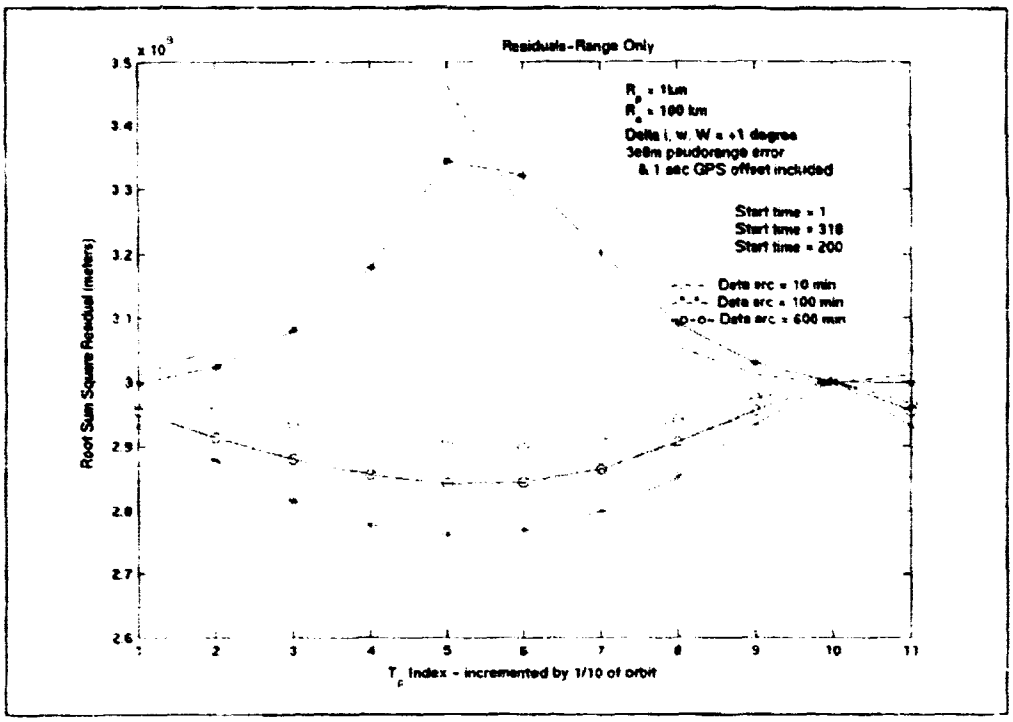


**Figure 8: RSS Residuals for IMEX Orbit with 1 s Clock Bias.** Graphs show multiple start times and data arcs for range residuals as a function of the assumed $\tau_p$.

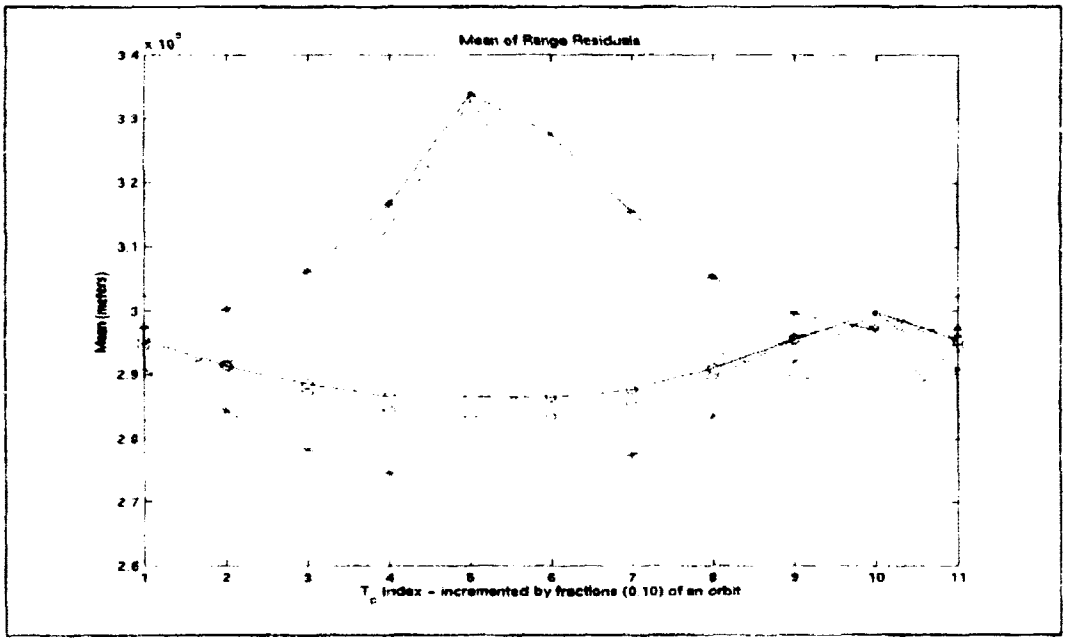


**Figure 9a: Mean of Range Residuals for IMEX Orbit with 1 s Clock Bias. Graph shows multiple start times and data arcs for range residuals as a function of the assumed $\tau_p$.**

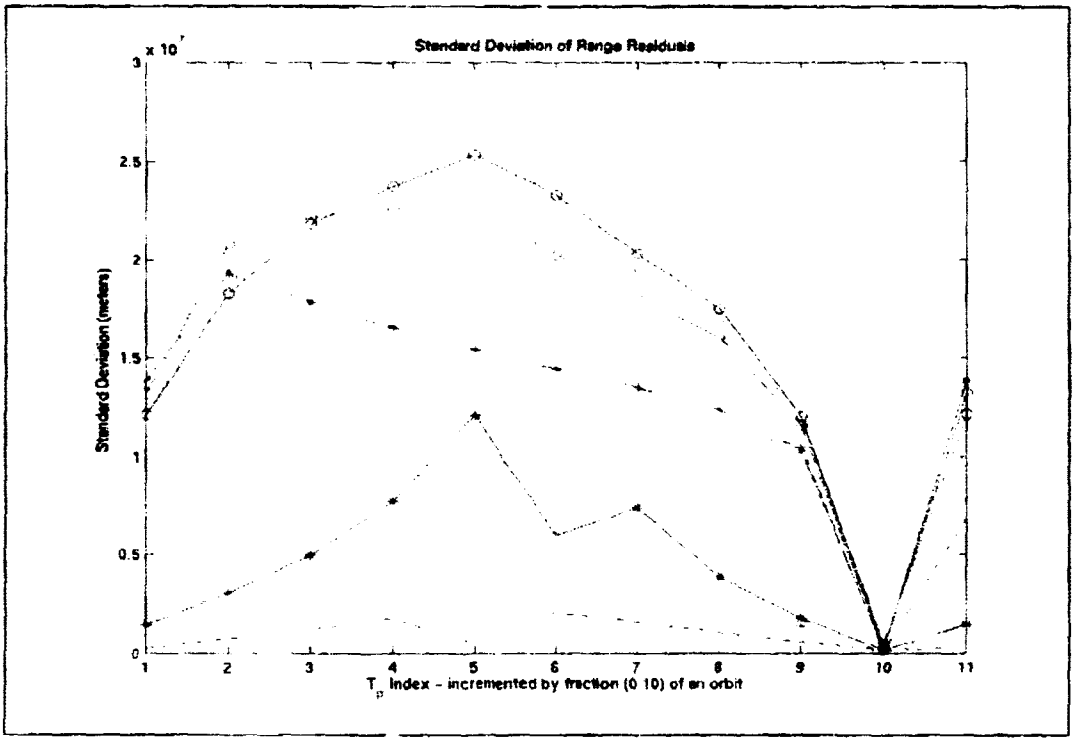


**Figure 9b: Standard Deviation of Range Residuals for IMEX Orbit with 1 s Clock Bias. Graphs show multiple start times and data arcs for range residuals as a function of the assumed $\tau_p$.**

**Table 4: Position and velocity estimation errors for batch initialization.** Initialization includes nominal orbit injection errors given in Table 1 for scenario 1. Results are shown for data arcs at perigee and apogee. Position and velocity errors in radial, in-track, and cross-track directions are given for the end of the data arc (100 minutes). The correct time of perigee passage is 38025 s.

| | Perigee data arc (1038 measurements) | | | Apogee data arc (982 measurements) | | |
|---|---|---|---|---|---|---|
| Search Increment | Tau Error (s) | Position Error RIC (m) | Velocity Error RIC (m/s) | Tau Error* (s) | Position Error RIC (m) | Velocity Error RIC (m/s) |
| 0.1 orbit (3803.8 s) | 130.929 | R = 3.52e4<br>I = 8.33e5<br>C = 4.99e5 | R = 72.38<br>I = 82.76<br>C = 60.9 | 130.929 | R = 1.64e5<br>I = 1.13e6<br>C = 5.9e5 | R = 31.51<br>I = 37.32<br>C = 35.38 |
| 0.01 orbit (380.38 s) | 16.46 | R = 2.54e5<br>I = 1.32e6<br>C = 5.06e5 | R = 1.346e2<br>I = 80.49<br>C = 59.80 | 92.77 | R = 1.24e5<br>I = 1.19e6<br>C = 5.95e5 | R = 41.33<br>I = 37.61<br>C = 35.59 |
| 0.00001 orbit (0.380 s) | 13.36 | R = 2.61e5<br>I = 1.36e6<br>C = 5.06e4 | R = 1.36e2<br>I = 80.43<br>C = 59.77 | 85.14 | R = 1.15e5<br>I = 1.20e6<br>C = 5.93e5 | R = 43.30<br>I = 37.67<br>C = 35.76 |

**Table 5: Position and velocity estimation errors for batch initialization.** Initialization includes nominal orbit injection errors of scenario 2, found in Table 1.

| | Perigee data arc (1038 measurements) | | | Apogee data arc (982 measurements) | | |
|---|---|---|---|---|---|---|
| Search Increment | Tau Error (s) | Position Error RIC (m) | Velocity Error RIC (m/s) | Tau Error* (s) | Position Error RIC (m) | Velocity Error RIC (m/s) |
| 0.1 orbit (3803.8 s) | 25.837 | R = 3.326e4<br>I = 5.197e4<br>C = 4.956e4 | R = .457<br>I = 8.41<br>C = 6.12 | 25.8 | R = 3.10e4<br>I = 9.14e4<br>C = 5.99e4 | R = 80.03<br>I = 93.61<br>C = 3.53 |
| 0.01 orbit (380.38 s) | 25.8 | R = 3.31e4<br>I = 5.20e4<br>C = 4.95e4 | R = .466<br>I = 8.40<br>C = 6.10 | 12.21 | R = 8.01e3<br>I = 1.15e5<br>C = 5.98e4 | R = 9.97<br>I = 3.64<br>C = 3.55 |
| 0.00001 orbit (0.380 s) | 15.94 | R = 6.93e3<br>I = 7.73e4<br>C = 4.96e4 | R = 5.97<br>I = 8.39<br>C = 6.11 | 8.714 | R = 1.30e4<br>I = 1.21e5<br>C = 5.89e4 | R = 4.48<br>I = 3.62<br>C = 3.54 |

**Initialization Results Analysis**

The initialization search procedure described within this memo was shown to be effective in location the position of a satellite within its orbit, based on GPS observations. The accuracy of the location is limited by the accuracy of the assumed orbit. Thus, if the errors in the nominal orbit elements are sufficiently small to initialized GEODE, this procedure allows you to solve for locations within the orbit to the same level of accuracy. As the estimates of the other elements have not been adjusted, the position and velocity estimates cannot be better than the a priori. For example, if the error in the assumed perigee is 10 km, the resulting perigee estimate cannot be better than 10 km, but we can determine if the satellite is at perigee.

Subsequently, based on these results, an additional step is required to develop a procedure to adjust all the element estimates based on the data so that the final position and velocity estimates are with in the convergence regime of GEODE.

# AMSAT DOPPLER PROCESSING

## 1. Introduction

The AMSAT OSCAR-40 (AO-40) spacecraft was launched into a highly elliptical orbit (HEO) in 2001. Although primarily designed to support amateur radio experiments, secondary experiments have been conducted to determine the feasibility of using GPS measurements for position and attitude determination in HEO. The satellite is in a low inclination, 1000 x 58,800 km altitude orbit, with an orbital period of approximately 19 hours. AO-40 uses an existing LEO GPS receiver, the Trimble TANS Vector, which poses significant operating limitations at high altitudes above the GPS constellation. However, the AO-40 experiment has already proven successful, achieving autonomous acquisition and tracking of GPS signals throughout the orbit, including signals with high dynamics around perigee and weak signals near apogee.

The TANS Vector reports several GPS observed variables, including code phase, carrier phase, and Doppler. Although the receiver is capable of returning position, velocity, and clock solutions when four or more GPS satellites are simultaneously tracked, no point solutions have been received to date. The primary tracking observable, pseudorange, can be constructed from the reported code phase. However, the lack of point solutions creates several unknowns, including satellite positions and clock biases, which make pseudorange recovery difficult.

The objective of our research was to utilize the returned Doppler measurements for post-processing orbit determination. Although Doppler solutions are generally less accurate, the Doppler measurements are less sensitive to the effects of the receiver, and may provide an initial estimation of the orbit from which to initialize other high fidelity post-processing schemes such as GEODE. Actual flight data from the receiver onboard AMSAT were processed in a Doppler-only batch filter. In addition, to further evaluate the performance of the filter and characterize unknowns within the flight data, simulated data were also processed

in the filter. This document reviews the Doppler-only batch algorithm, and presents the results from actual and simulated data processing.

## 2. Batch Approach

We implemented a traditional batch filter to process the Doppler measurements, the basis of which is similar to the batch described for the initialization algorithm. The filter is utilized to process AMSAT flight data, consisting of returned Doppler data, as well as simulated data, based on generated satellite positions and velocities.

This approach assumes an initial 'truth' vehicle state, and propagates through the orbit to each of the measurement times. Initially, this propagation uses a purely Keplerian model without considering perturbation effects. Estimated range-rates are computed from the propagated satellite positions and velocities, and the GPS satellite positions determined from the broadcast ephemeredes. The estimated range-rate is compared with either the measured Doppler converted to range-rate, or a simulated range-rate to produce measurement residuals for the entire arc of data. A least squares solution is performed to produce an updated estimate of initial satellite position and velocity, and iterations are performed until the updated estimate and the initial truth match within tolerances. This simple filter was additionally updated to consider measurement weighting based on *a priori* information. The results of both the simple filter and the weighted batch filter are presented and compared.

### 2.1 State Parameters

The vehicle state is comprised of position, velocity, and frequency bias.

$$X = \left[ R_1 \; R_2 \; R_3 \; \dot{R}_1 \; \dot{R}_2 \; \dot{R}_3 \; f \right]$$

Initially, time tag error, TE, was also included in the estimated state. However, further analysis of the Doppler measurement partials indicated that the sensitivity of range-rate to

time tag error is low (1 sec TE ~ 10 cm/s range-rate). With time tag errors expected to be fairly small, adequate solutions should be achievable without TE estimation, and therefore it was not considered in the final solution.

### 2.2 Measurements

GPS Receiver 1 onboard AO-40 was first operated from September 25th through November 2nd, 2001. This receiver uses a blind search technique, sequentially searching though the possible GPS satellite PRNs to acquire and track GPS satellites. The most promising batch of data was obtained on October 5th, on a pass near perigee were 4 satellites appear to be tracked simultaneously, although point solutions were not returned. The receiver forms Doppler measurements for each satellite tracked, which are provided at approximately half-second intervals. A 15 minute arc of data with 5 total PRNs tracked around the perigee pass was considered. The observed Doppler measurements were converted to range-rate measurements for processing in the filter.

Simulated observations were also constructed for the same arc of data using satellite positions and velocities generated in STK. The measured range-rate was constructed from a non-linearized true range-rate model plus a random error.

## 3. Data Processing

The batch algorithm used a MATLAB simulation environment to post-process both the flight data and the simulated STK data, the components of which are described below.

### 3.1 Reference Trajectory

The reference trajectory for AO-40 was generated from a NORAD Two-Line Ephemeris (TLE), for October 5th, 2001 using STK's MSGP4 (Merged Simplified General Perturbations) propagator. This high fidelity propagator considers secular and periodic

variations due to J2, solar and lunar effects, and atmospheric drag. The position and velocity at the initial measurement time are pulled from this reference trajectory and used as the initial state estimate in the batch propagator.

## 3.2 Measurement models

The batch filter utilizes the same process to generate computed measurements for both AMSAT flight data and simulated data scenarios. However, computations for observed measurements for each scenario differ slightly, and will be discussed separately.

### 3.2.1 Computed Measurements

a) Initial state estimate from the STK reference trajectory is propagated to each of the measurement times using a 2-body propagator.
b) The estimated positions and velocities, and GPS positions and velocities are used to generate an estimated range-rate at each of the measurement times, based on a non-linear Doppler model.
c) Estimated range-rates are calculated similarly for both flight data and simulated data scenarios

### 3.2.2 Observed Measurements

AMSAT Flight Data

a) The batch filter selects the Doppler measurement and converts to a range-rate measurement by multiplying by the negative L1 wavelength.

STK Simulated Data

b) The measured range-rate is derived from the reference trajectory.
c) The reference positions and velocities at each measurement time are used with the GPS positions and velocities to generate a 'true range-rate'.
d) A random noise (few m/s) is then added to each true measurement to create a measured range-rate.

## 3.3 Doppler-only Batch Algorithm

a) Determine reference trajectory in using a TLE in STK
b) Compute AMSAT R/V at the measurement time based on the *a priori* $R_o/V_o$ from reference trajectory propagated in the 2-body propagation algorithm
c) Calculate the estimated range-rates

Estimated LOS:

$$LOS_{est} = R_{GPS} - R_{AMSAT}$$

Estimated Range:

$$\rho_{est} = \sqrt{(LOS^2)}$$

Estimated Range-rate:

$$\dot{\rho}_{est} = \left(\frac{LOS_{est}}{\rho_{est}}\right)\left(\frac{V_{GPS} - V_{AMSAT}}{1 - \left(\left(\frac{LOS_{est}}{\rho_{est}}\right)\left(\frac{V_{GPS}}{c}\right)\right)}\right)$$

d) Determine measured range-rates

a. For AMSAT flight data:

Measured range-rate:

$$\dot{\rho}_{meas} = -(Dop_{meas})(\lambda_{L1})$$

b. For simulated data

True range-rate:

$$\dot{\rho}_{true} = \left(\frac{LOS_{true}}{\rho_{true}}\right)\left(\frac{V_{GPS} - V_{REF}}{1 - \left(\left(\frac{LOS_{true}}{\rho_{true}}\right)\left(\frac{V_{GPS}}{c}\right)\right)}\right)$$

Measured range-rate:

$$\dot{\rho}_{meas} = \dot{\rho}_{true} + random\ noise$$

e) Compute Doppler-only measurement residuals

$$\dot{\rho}_{meas} - (\dot{\rho}_{est} + \dot{f})$$

f) Form H matrix

$$\left[\frac{\partial\dot{\rho}}{\partial R} \quad \frac{\partial\dot{\rho}}{\partial V} \quad 1\right]$$

$$\left[\frac{-V_{AMSAT} + \left(\dot{\rho}_{est} * \frac{LOS_{est}}{\rho_{est}}\right)}{\rho_{est}} \quad -\frac{LOS_{est}}{\rho_{est}} \quad 1\right]$$

g) Accumulate measurement residuals and H matrices for all measurement times.
h) Solve for the state correction, *dx*.

$$dy = H*dx$$

i) Update the initial position/velocity with *dx*, iterate.

## 4. Data Processing and Results

AMSAT FLIGHT DATA

Actual Doppler data consisting of a fifteen minute arc near perigee were processed in the batch filter, summarized in Table 1.

**Table 1: Flight Data**

| Date | Start SOW | End SOW | Data Rate | Satellites | Notes |
|---|---|---|---|---|---|
| 10.05.01 | 493194.2513 | 494096.75 | ~ 0.5 seconds | 3, 11, 22, 25, 31 | Near perigee, 4 simultaneous |

An initial state estimate from STK was propagated to the measurement times using the Keplerian propagator. Other perturbations were not considered. Additionally, *a priori* weighting of the data was not considered. The batch filter estimated values of $\hat{R}_o, \hat{V}_o, \hat{f}$, and the observed minus computed measurement residuals were examined over several iterations to evaluate the performance of the filter.

Initially, examination of the residuals for the first two iterations indicates that the filter is adjusting the estimates properly. The residuals begin to converge to a zero value as expected, shown in Figure 1. In addition, the filter appears to attempt to converge over the next 10 iterations. The values of $\hat{R}_o, \hat{V}_o, \hat{f}$, appear to converge to appropriate values, while the state correction value, $dx$, for each variable converges on zero as anticipated, shown in Figures 2, 3 and 4 respectively. Figure 5 illustrates the residuals over these 10 iterations.

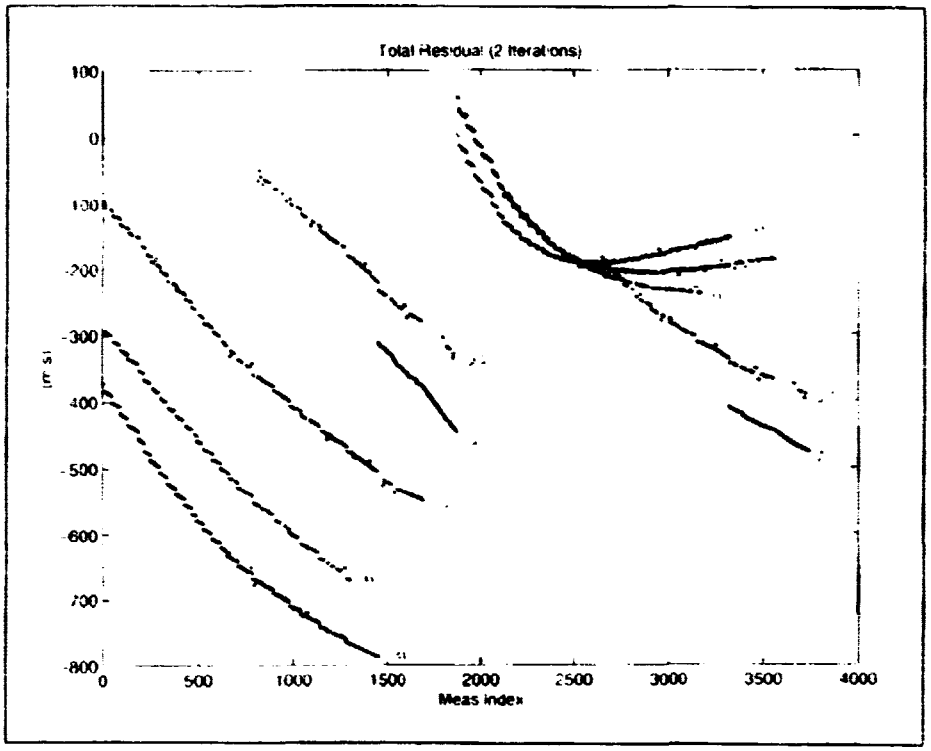


**Figure 1: Measurement Residuals by PKN for First 2 Iterations**

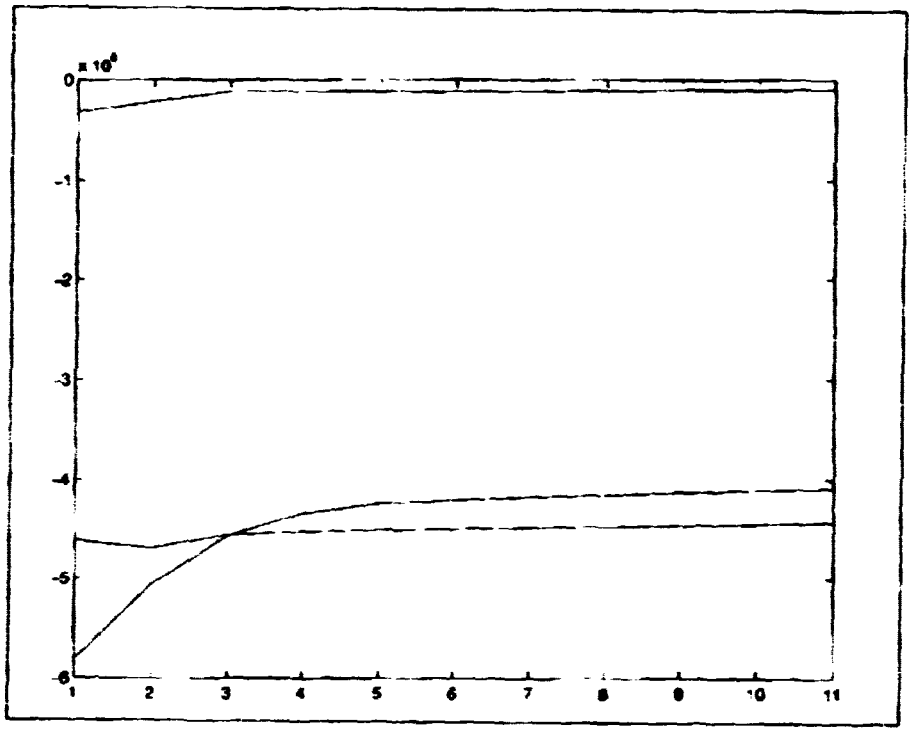


**Figure 2 (a): Ro (X Y Z) over 10 iterations (m)**

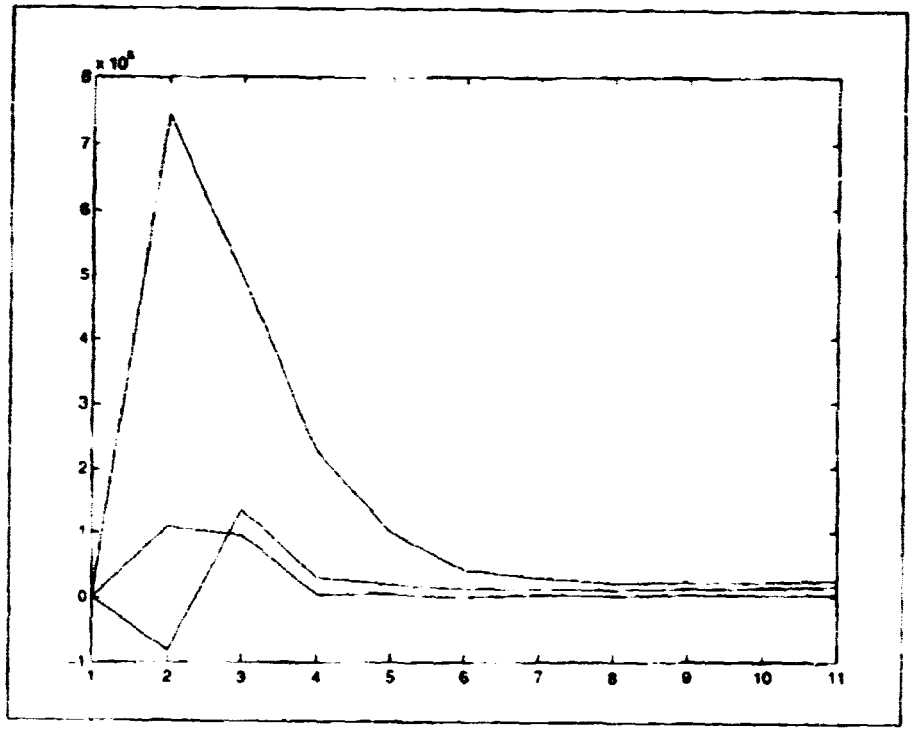


**Figure 2 (a): Position correction, dR, for 10 iterations (m)**

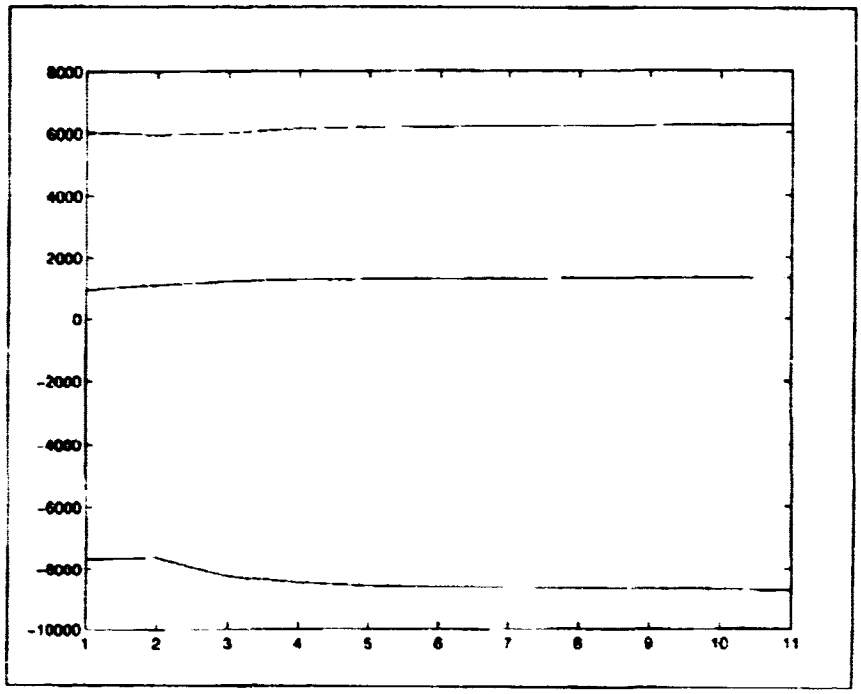


**Figure 3 (a): Vo (XYZ) for 10 iterations, (m/s)**

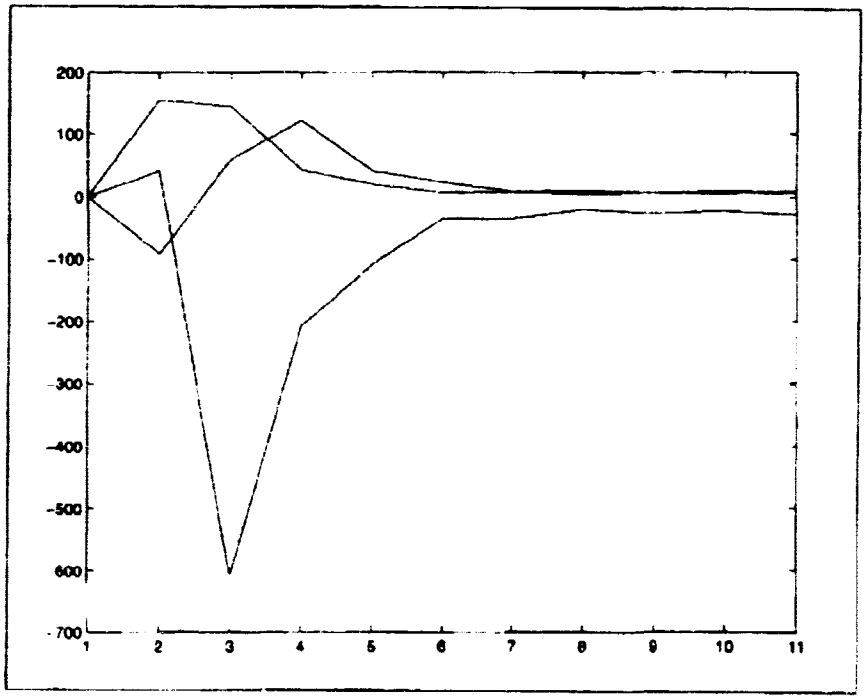


**Figure 3 (b): Velocity correction. dV, for 10 iterations. (m/s)**

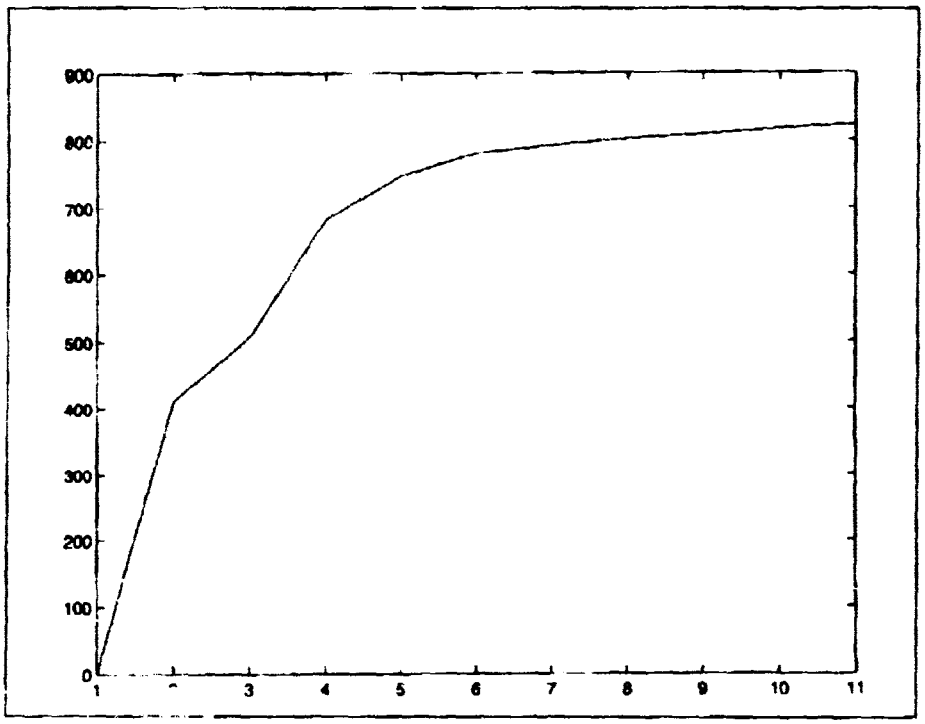


**Figure 4 (a): Frequency bias estimate (m/s), 10 iterations**

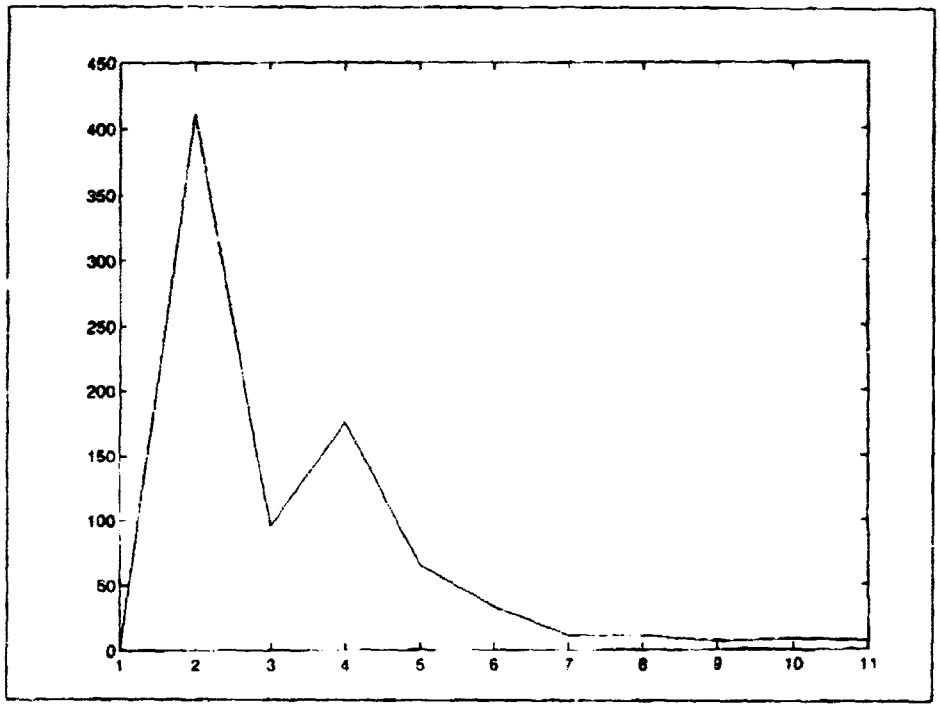


**Figure 4 (b): Frequency bias correction (m/s), 10 iterations**

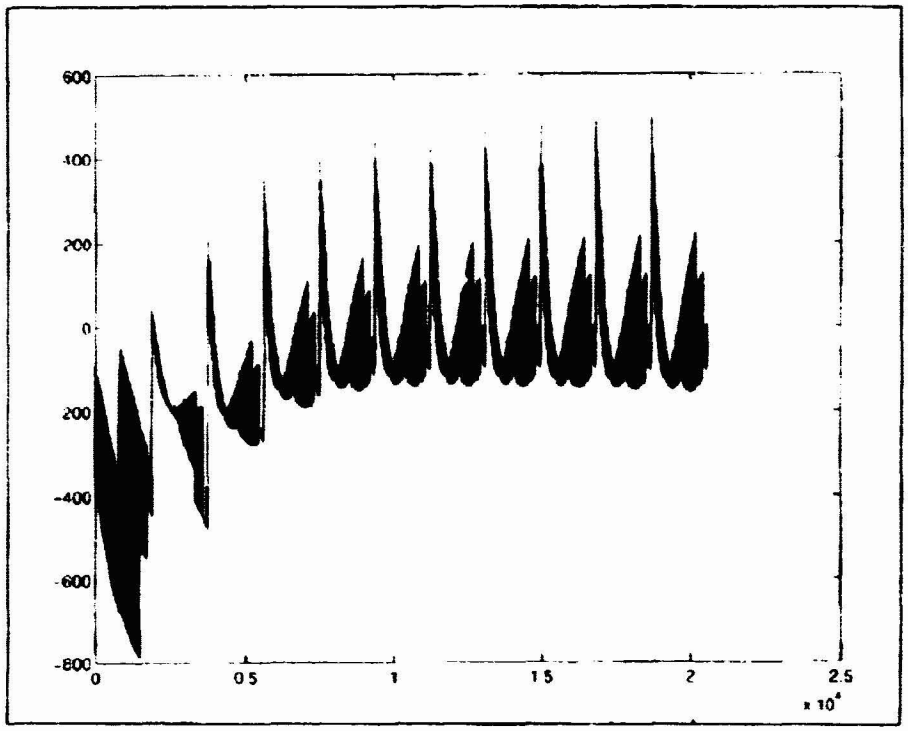


**Figure 5: Measurement Residuals (m/s), 10 iterations**

Although evaluations of the state parameters indicate that the filter is slowly trending toward convergence, examination of the residuals reveal potential problems. Although the residuals appear to center around a zero value, the filter appears unable to converge the measurements from each separate GPS satellite. Further, additional iterations do not continue the trend towards convergence, and a suitable solution is not obtained. Instead the filter appears to become unstable, with the residuals becoming very large at approximately 20 iterations, as shown in Figure 6.

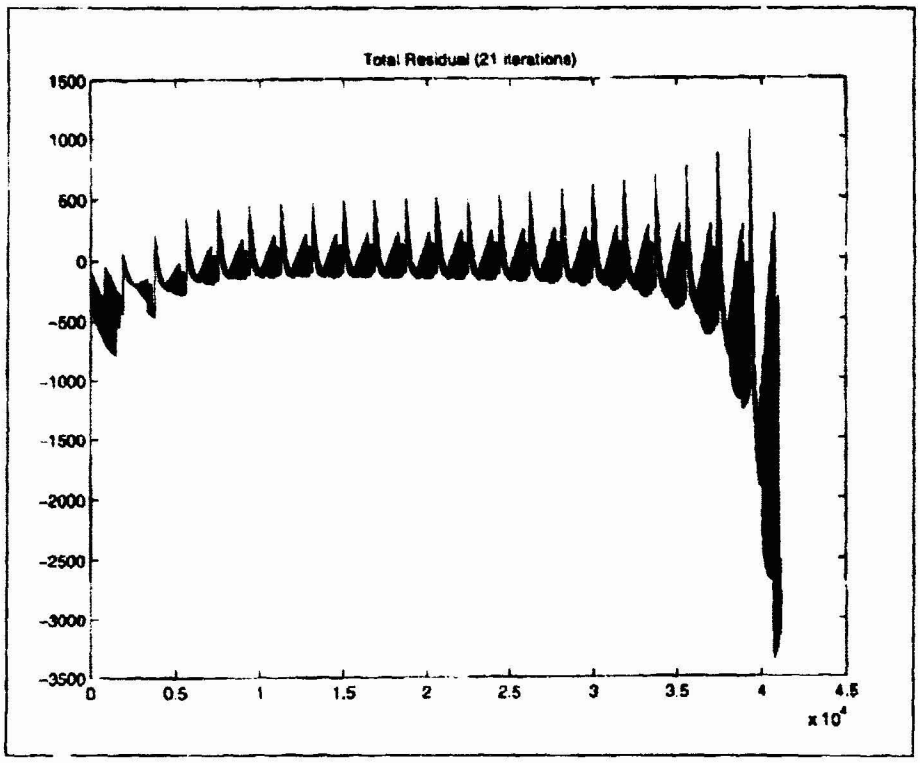


**Figure 6: Measurement Residuals (m/s), 21 iterations.**

Initially, we considered the possibility that improper measurement weighting contributed to the lack of convergence and ultimate failure of the filter in the previous scenario. To examine this further, the filter was expanded to incorporate *a priori* covariance and weighting estimations. The general solution of this weighted least-squares filter is shown below.

$$Solve \quad L * \hat{x}_o = N \; for \; dx$$

$$where \quad L = \overline{P}_o^{-1} + \sum HWH \quad and \quad N = \overline{P}_o^{-1} * dx + y$$

P – covariance matrix

W – weighting matrix

$x_0$- initial state deviation, or correction

However, multiple attempts to adjust the weighting and *a priori* covariance did not appear to correct the filter divergence, as shown in Figure 7.

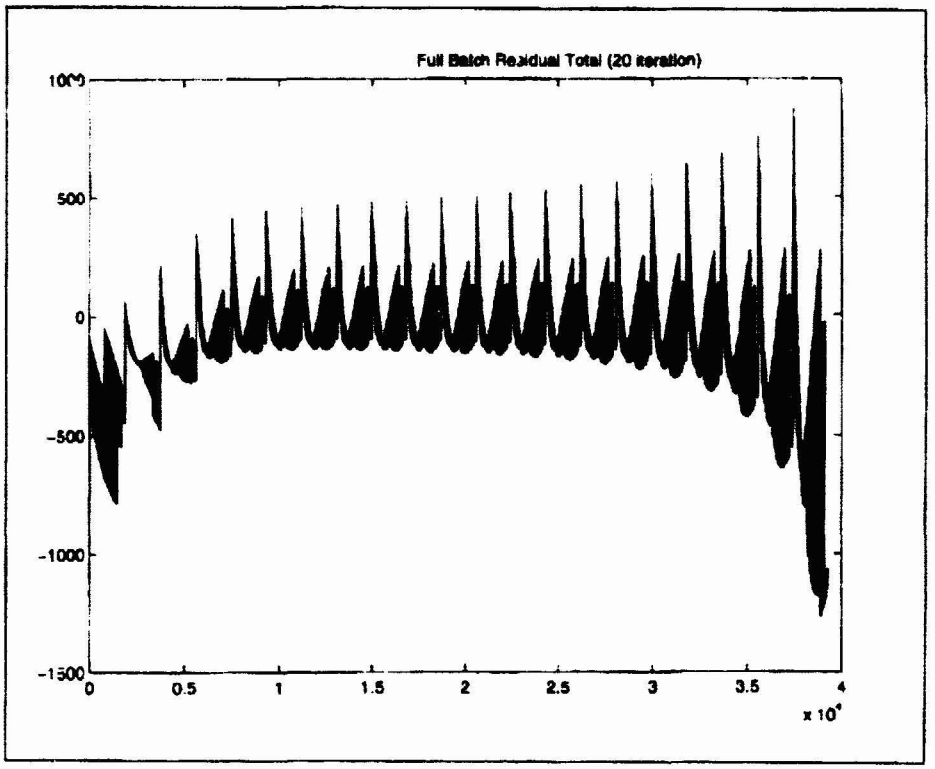


**Figure 7: Measurement Residuals for Weighted Least-Squares Filter (m/s), 20 Iterations**

Several unknowns exist with the flight data that could contribute to the failure of the filter. These include bad data related to one or more PRNs, poor geometry of the GPS satellites, not enough data in the batch, and unmodeled noise within the data. To examine these possibilities, we constructed simulated data with fewer unknown error sources for the same batch. The results of processing these data are discussed below.

## STK SIMULATED DATA

Using the positions and velocities from the reference trajectory, truth range-rate measurements were computed. To these we added a measurement error of less than $1\sigma$ to generate the 'observed' measurements. An offset of 1% in semi-major axis and eccentricity was added to the initial state estimate from the reference trajectory from which the estimated AMSAT positions, velocities and range-rate measurements were calculated. Additional parameters,

such as number of satellites, data rate and total batch size remained the same as in the flight data scenario.

Figure 8 illustrates the measurement residuals for the simulated data after 20 iterations. Figures 9(a) and (b) show the state corrections, dR and dV, for each iteration. It is clear that the filter is able to process the data successfully, converging on a suitable solution after approximately eight iterations.

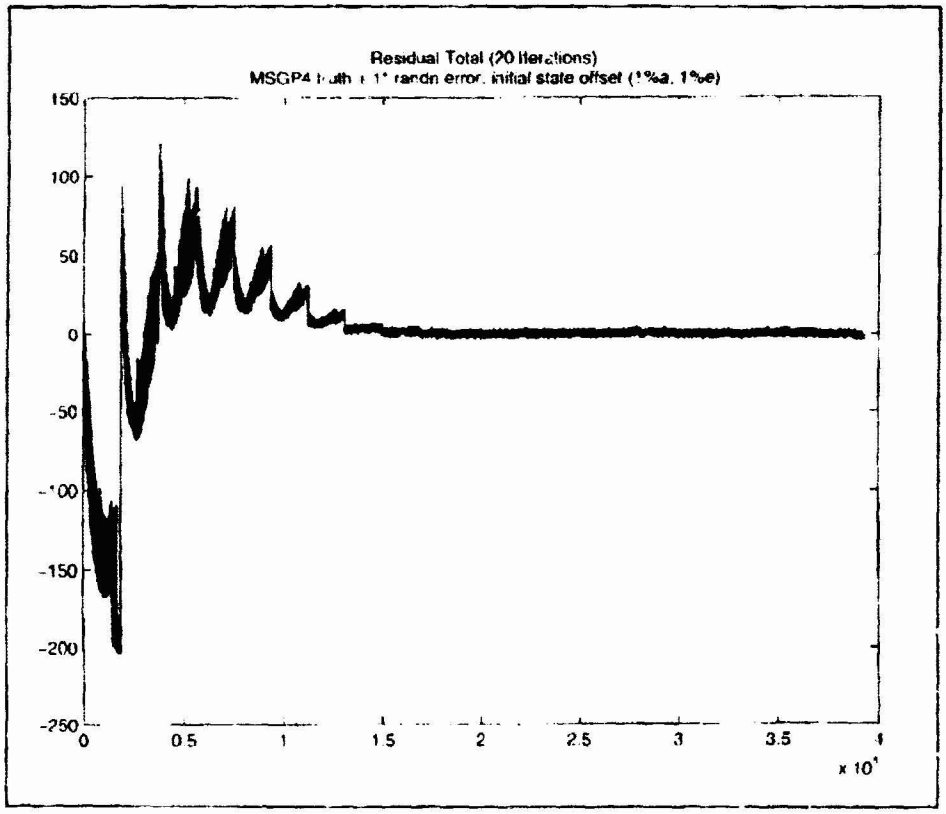


**Figure 8: Measurement Residuals for Simulated Data (m/s), 20 iterations**

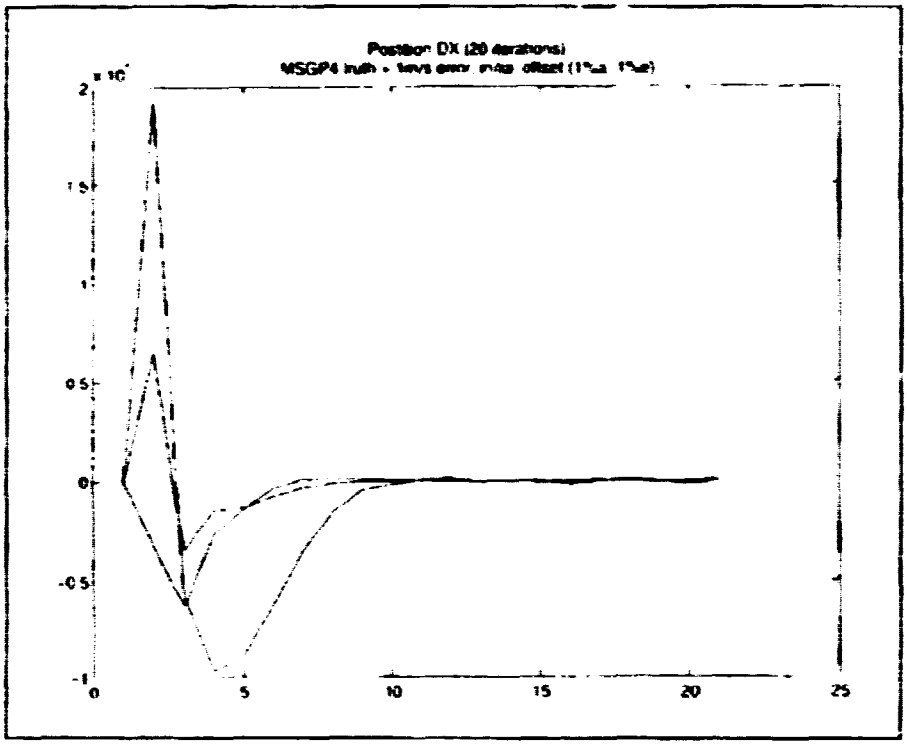


**Figure 9 (a): Position DX (XYZ) for Simulated Data (m), 20 iterations**

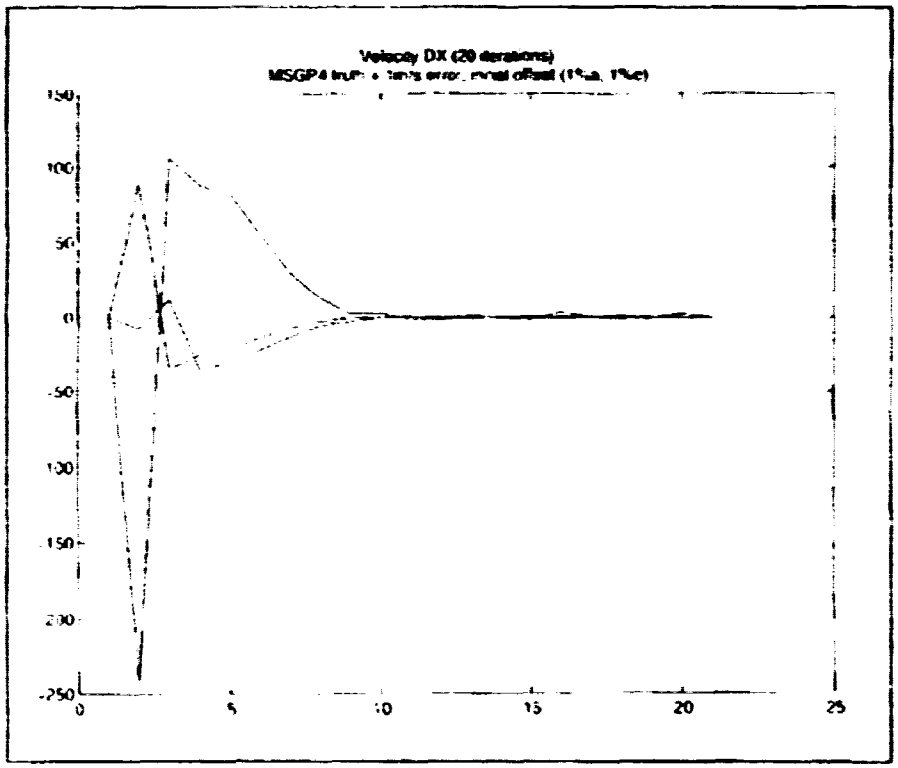


**Figure 9 (b): Velocity DX for Simulated Data (m/s), 20 iterations**

Table 2 contains the initial offset values, the final values for the state estimate at epoch, $R_o$,$V_o$, as well as the difference between the final solution and truth after 20 iterations.

**Table 2: Simulated Data Results**

| Initial Offset (1% a, 1% e) Position (m) | Initial Offset (1% a, 1% e) Velocity (m/s) | Estimated Initial Position ($R_o$) | Estimated Initial Velocity ($V_o$) | Truth-Est Position (m) | Truth-Est Velocity (m/s) |
|---|---|---|---|---|---|
| -1.694 e5 | -4.4 e2 | -5.807e6 | 6.048e3 | 34.76 | .491 |
| -1.35 e5 | 5.6 e2 | -4.607e6 | -7.67e3 | 86.60 | .831 |
| -.093 e5 | -0.2 e2 | -0.321e6 | 0.946e3 | -397.3 | -.257 |

These results clarify several concerns. First, it verifies the filters ability to process data correctly, and rules out any errors in software or the algorithm. More importantly, it indicates that both the geometry of the GPS satellites, as well as the amount of data processed is sufficient for filter stability and convergence. Given this, it seems likely that the filter fails on the actual flight data because of unknown and therefore poorly modeled errors or noise in the Doppler data. It is interesting to note that the filter will fail with the simulated data if too much measurement noise (more than a few m/s) is added. Actual flight data are expected to have more measurement noise, therefore we reasonably believe this is one specific cause of filter failure on the AMSAT data.

## 5. Future Studies

Goddard Space Flight Center has generated additional data using an actual TANS Vector receiver in a high fidelity flight simulator for the Landsat 7 orbit (LEO). Again, being simulated, these data have fewer unknowns within the scenario, and therefore can be used to examine the function of the receiver itself and the quality of the data generated. Preliminary attempts to process these data in the Doppler-only batch were performed to further determine what elements within the flight data from this receiver create divergence in the filter.

Simple studies using STK indicate that effects from the oblateness of the Earth, J2, are more pronounced with a LEO orbit than with a HEO, as expected. Figure 10 compares the Landsat 7 orbit propagated with a 2-body propagation verses propagated with J2 effects included. The errors resulting from a 2-body propagation in LEO indicate that the Keplerian propagator

originally in the filter would not produce a sufficient estimated trajectory. The filter propagator was therefore replaced with a fourth order Runga-Kutta integration propagator with equations of motion that include effects of J2 and atmospheric drag.

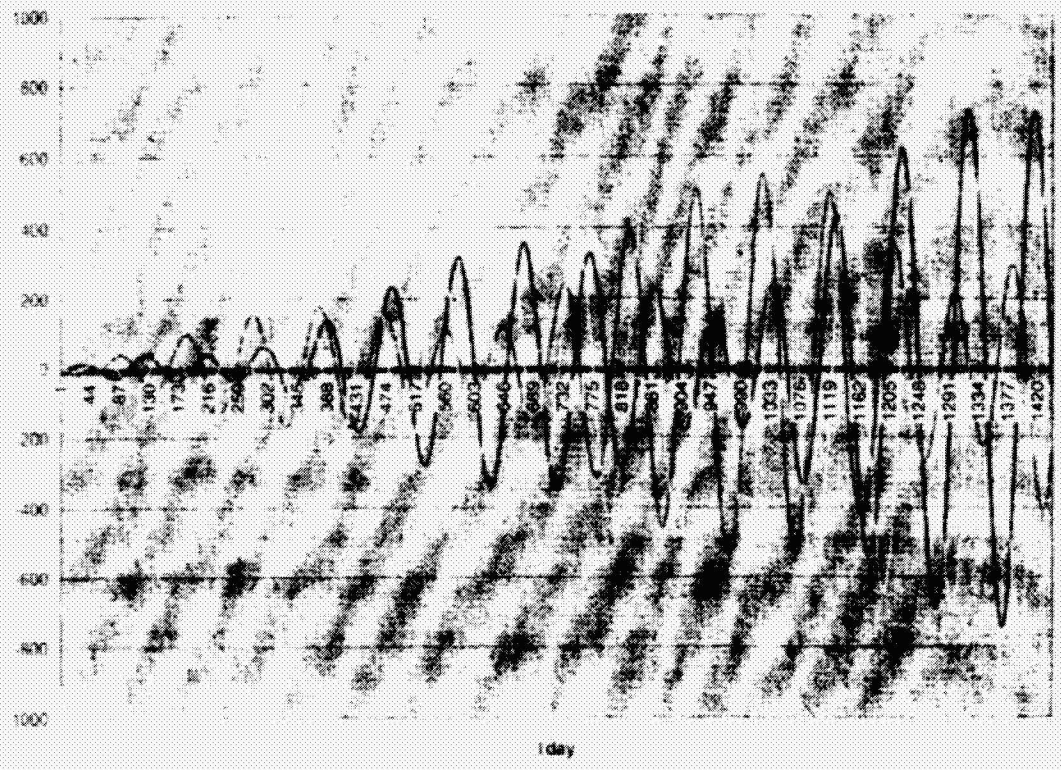


**Figure 10: J2 Minus 2Body Propagation, LS7 (km)**

Initial attempts to process the LS7 data in the new filter have not been successful. The primary difficulty appears in the propagation of the estimated orbit, which rapidly diverges away from the truth trajectory, as indicated in Figure 11. It can be seen that after approximately 100 measurements, the in-track position of the estimated orbit steps and then rapidly diverges from the truth in-track position. The same trend can be seen in the radial velocity.

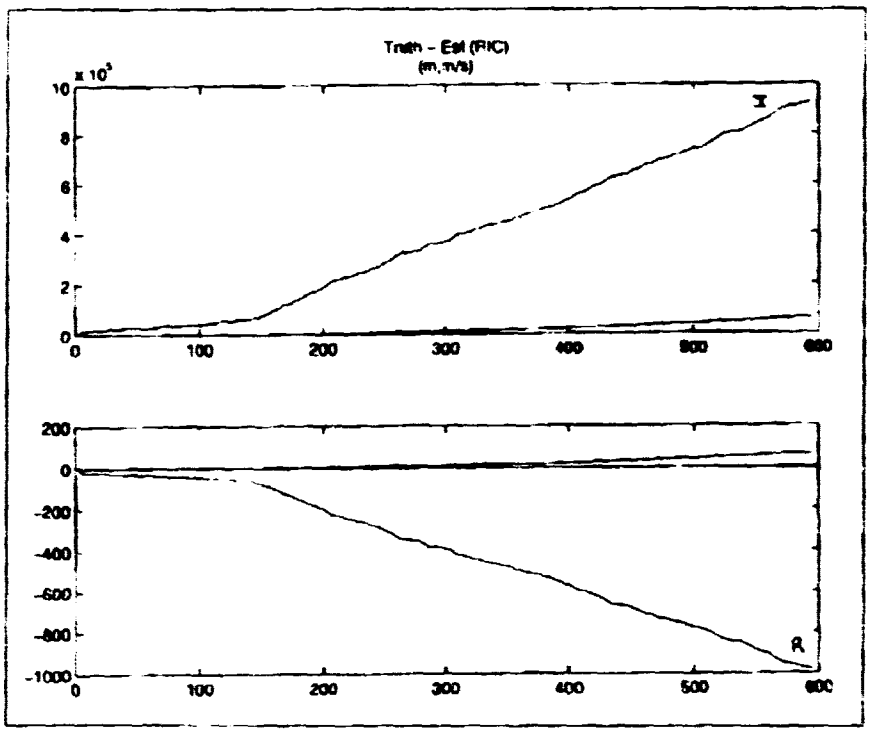


**Figure 11: Truth Orbit - Estimated Orbit (RIC), LS7 (m, m/s)**

This propagator has successfully generated orbits for other similar orbit scenarios, so it is unclear why these trends are seen with the Landsat 7 orbit. It is believed that there may be a coordinate system difference between truth and the estimated orbit, but this has not been confirmed. Successful testing with this data set could be extremely useful in understanding the data returned from the TANS Vector, and for further post-processing attempts of data from AMSAT.

**Results Analysis**

The Doppler-only batch procedure described was shown to be effective in post-processing orbit determination for the simulated AMSAT orbit, based on generated measurements and visible GPS satellite information. AMSAT flight data have yet to be filtered successfully, believed in part to be due to noise and additional unknown errors in the flight environment and with the TANS Vector receiver itself. Successful testing with the Landsat 7 data set could

be extremely useful in understanding the data returned from the TANS Vector, and in further post-processing attempts of data from AMSAT.

**Additional Sources and Acknowledgements:**

Davis, George. "GPS-Based Navigation and Orbit Determination for the AMSAT AO-40 Satellite". AIAA

Moreau, Michael, et al. "Preliminary Results of the GPS Flight Experiment on the High Earth Orbit AMSAT-OSCAR 40 Spacecraft". *AAS Guidance and Control Conference, Breckenridge, CO, February 2002.*

Several people have supported the efforts on these projects. The contributions of Mike Moreau, Russell Carpenter, and Anne Long at NASA GSFC are greatly appreciated.